



Recovery of sulphur dioxide by converter dust synergistic coke decomposition of phosphogypsum

Dong Ma, Qinhui Wang^{*}, Zhihua Tian, Bin Zhang, Guilin Xie

State Key Laboratory of Clean Energy Utilization, Institute for Thermal Power Engineering, Zhejiang University, Hangzhou 310027, China

ARTICLE INFO

Keywords:

Phosphogypsum
Coke
Converter dust
Sulfur dioxide
Recovery

ABSTRACT

To further improve the decomposition ratio and sulfur dioxide mass yield of coke-reduced solid waste phosphogypsum (PG), converter dust (CD) is proposed as a novel additive. The effects of raw material ratio, time and temperature for roasting on the decomposition process of PG were inspected by simulation calculations and fluidized bed experiments. It turns out that the optimized reaction conditions are $\text{Fe}_3\text{O}_4/\text{Ca}$ of 0.6, C/Ca of 0.4 at $1100\text{ }^\circ\text{C}$ for 24 min, under which the PG decomposition ratio and SO_2 mass yield are 99.56 % and 97.64 %, respectively. The addition of CD is able to reduce the initial reaction temperature from $975\text{ }^\circ\text{C}$ to $914\text{ }^\circ\text{C}$, and promote the release of SO_2 . Kinetic analysis shows the mechanistic equation for this process is obtained as $G(\alpha) = [-\ln(1 - \alpha)]^{3/2}$, indicating that the decomposition reaction mechanism is a crystal nucleation and growth-controlled process. The chemical mechanism of the process is that coke and Fe_3O_4 in the CD convert CaSO_4 to the intermediate CaS, and Fe_3O_4 is oxidized to Fe_2O_3 . Then CaS and CaSO_4 continue to react with Fe_2O_3 to form $\text{Ca}_2\text{Fe}_2\text{O}_5$ and SO_2 . The presence of Fe_2O_3 accelerates the rate of CaS and CaSO_4 roasting reaction and lowers the reaction temperature. Meanwhile, the self-decomposition of PG also produces CaO and SO_2 . Finally, a process for SO_2 recovery from CD synergized with coke decomposition of PG is proposed.

1. Introduction

Phosphogypsum (PG) is a solid waste from the treatment of phosphate rock with sulfuric acid in the production of phosphoric acid. $\text{CaSO}_4 \cdot 2\text{H}_2\text{O}$ is the main ingredient in PG. Additionally, it contains impurities including Si, P, and F (Qi et al., 2023). The presence of contaminants inhibits the use of PG on a big scale. It is estimated that every 1 ton of phosphoric acid produced will produce 5 tons of PG (Ennaciri and Bettach, 2018). At present, China's PG storage capacity has exceeded 250 million tons, and the annual output is maintained at 75–78 million tons, but the utilization rate of resource utilization is only about 40 % (Chen et al., 2023). Currently, PG is mainly disposed of by stockpiling. However, stockpiling not only results in a large amount of occupied land, but also is highly susceptible to contamination of the atmosphere and groundwater (Silva et al., 2022). Therefore effective treatment of PG is urgent.

The solution to this issue is the thermochemical reduction of PG into calcium oxide and sulfur dioxide at high temperatures. Calcium oxide can be used as a source of raw materials for building supplies and sulfur dioxide can be used to make sulfuric acid (Atanasova, 2010). This

process can transform trash into treasure, reduce environmental pollution from PG, and partially replace sulfur in the process of making sulfuric acid. Reductants are used to lower the PG initial reaction temperature. The reductants that have been reported so far are lignite (Ma and Wang, 2023), bituminous coal (Zheng et al., 2013), high-sulfur coal (Zheng et al., 2011), char (He et al., 2023), biomass (Ma et al., 2023), biochar (Luo et al., 2023), sulfur (Chen et al., 2021), FeS_2 (Fang et al., 2020), sulfurous iron ore (Liu, xxxx), H_2S (Ji et al., 2023), CO (Liu et al., 2023) and H_2 (Jia et al., 2023). Reductants reduces the self-decomposition temperature of PG from $1150\text{--}1200\text{ }^\circ\text{C}$ to $850\text{--}900\text{ }^\circ\text{C}$. To further lower the reaction temperature while increasing the products yield, on the basis of the reductants, the researchers proposed the addition of suitable additives. The main additives that have been reported so far include FeCl_3 (Zheng et al., 2018), Fe_2O_3 (Yang et al., 2019), iron-phosphorus slag (Sun et al., 2022), Al_2O_3 (Zhao et al., 2015), SiO_2 (Shi et al., 2016), potassium feldspar (Lu et al., 2021). The Fe-based additives in the PG thermal decomposition is the most widely used, the most intensively researched, and the most effective. However, the currently studied iron-based additives are mainly formed by post-processing, which is not economical in terms of resource utilization.

^{*} Corresponding author.

E-mail address: qhwang@zju.edu.cn (Q. Wang).

<https://doi.org/10.1016/j.ces.2024.119814>

Received 20 September 2023; Received in revised form 4 January 2024; Accepted 22 January 2024

Available online 23 January 2024

0009-2509/© 2024 Published by Elsevier Ltd.

Table 1

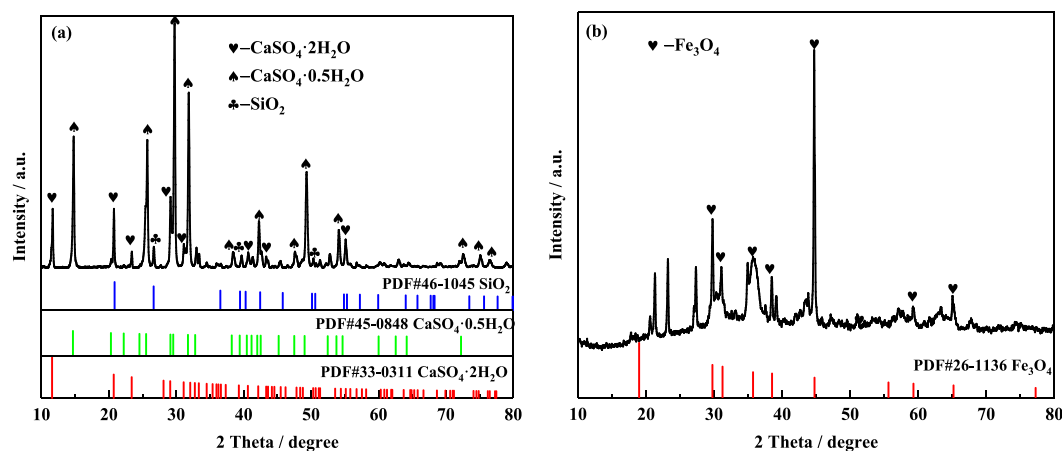
Primary chemical components of PG / %.

SO ₃	CaO	SiO ₂	P ₂ O ₅	MgO	Fe ₂ O ₃	F	Na ₂ O	TiO ₂	K ₂ O	Al ₂ O ₃	Water of crystallization
43.12	30.28	5.42	0.87	0.21	0.17	0.16	0.09	0.08	0.01	–	12.21

Table 2

Primary chemical components of CD / %.

Fe ₂ O ₃	CaO	K ₂ O	ZnO	SiO ₂	Na ₂ O	Al ₂ O ₃	MgO	P ₂ O ₅	SO ₃	PbO
72.46	7.65	4.38	3.62	2.67	1.35	1.48	1.64	0.23	0.48	0.05

**Fig. 1.** Mineral ingredients of raw materials: (a) PG, (b) CD.

Therefore, the use of widely available industrial solid wastes that do not require post-processing instead of conventional additives that need to be prepared can maximize resource utilization.

Converter dust (CD) is a solid particle collected after the flue gas is purified by a dry de-dusting system during the steelmaking process in a converter. Each ton of steel produces about 20 kg of CD, and the iron and steel sector in China produces roughly 0.2 billion tons of CD each year (Zhou et al., 2022). The main constituent of CD is Fe₃O₄ (Da Rocha et al., 2013). If Fe₃O₄ in CD can be utilized instead of conventional Fe additives to promote the decomposition process of PG, this not only promotes the resourceful use of PG and CD, but also saves resources. There hasn't been any information published on the research of CD as an additive to decompose PG. Therefore, in this paper, for the purpose of reducing PG to recover SO₂, the impact of CD on the coke reduction PG is studied. On the process, the impacts of raw material ratios and roasting temperatures are examined by HSC thermodynamic equilibrium calculations combined with fluidized bed experiments and kinetic analyses in order to optimize the roasting conditions.

2. Raw materials and procedure

2.1. Materials

CD and PG are supplied by a steel smelting industry and a phosphorus chemical industry respectively. The PG and CD are sieved, and

Table 3

Lignite and coke characteristics / %.

Materials	M _{ad}	FC _d	A _d	V _d	S _{t,ad}	H _{ad}	N _{ad}	C _{ad}	O _{ad} [*]
Lignite	5.07	34.54	46.62	18.84	0.56	4.45	1.33	54.10	20.72
Coke	1.23	70.75	27.83	1.42	0.23	0.31	0.86	68.36	2.41

*By difference. M_{ad}- Air dry base moisture, FC_d- dry basis fixed carbon, A_d- dry basis ash, V_d- dry basis volatiles, S_{t,ad}- air dry basis total sulfur, H_{ad}- air-drying base hydrogen, N_{ad}- air-drying base nitrogen, C_{ad}- air-drying base carbon, O_{ad}- air drying oxygen.

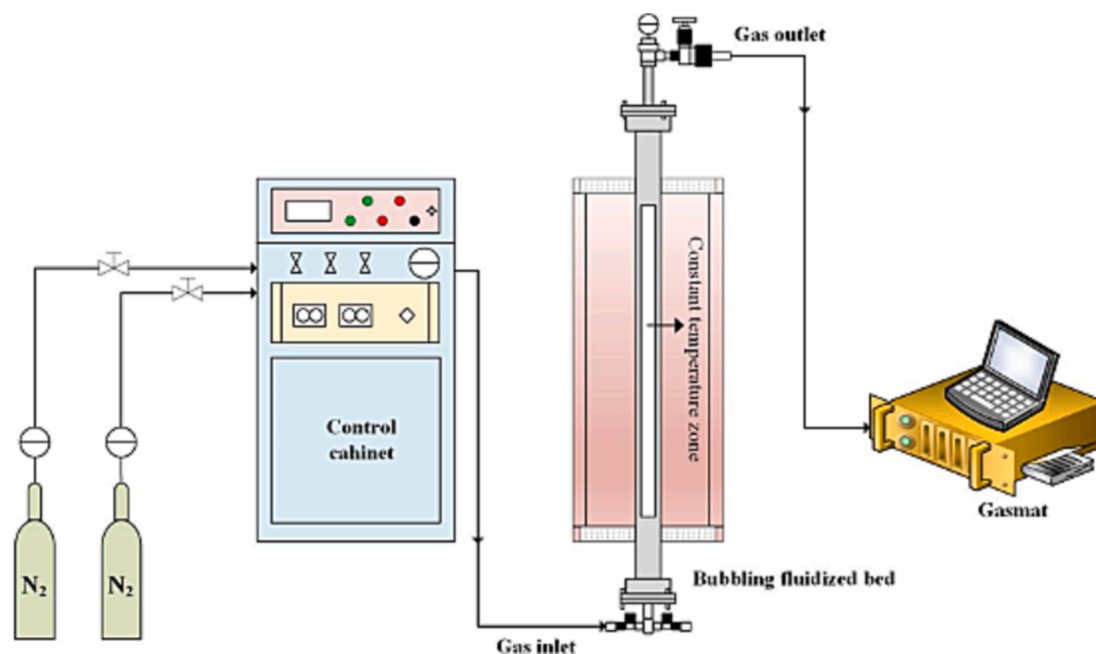


Fig. 2. Small bubbling fluidized bed experimental setup diagram.

2.2. Experimental steps

The fluidized decomposition method is the primary experimental technique employed in this investigation. Fig. 2 shows the experimental platform. A control device, a heating device, and a gas online analysis equipment are the major components of the experimental system. It can realize the sampling of solid products and the analysis of gas products. A quartz tube reactor with a length of 1.5 m and an inner diameter of 50 mm is mounted in the center of the heating unit. The experimental procedure is batch feeding, 2 g of PG is weighed before the start of the experiment, coke and CD are weighed according to the C/Ca ratio and $\text{Fe}_3\text{O}_4/\text{Ca}$ ratio, respectively. Materials are mixed well and then placed in a bin with a sieve, which is then placed into the top of the reactor. The quartz tube reactor is heated electrically to the desired temperature, while air is then forced out of the tube using N_2 . Once the temperature is reached and stabilized, a feeding mechanism is used to add the sample to the reactor. The flue gas composition at the furnace outlet is online analyzed using a flue gas analyzer. The gas is then put into a gas bag for storage. After reaching the set thermostatic time, the reaction products are removed from the reactor when the temperature is reduced to room temperature, cooled down and packed in sealed sample bags for later analysis and calculation.

2.3. Methods of analysis

The BaSO_4 gravimetric method (GB/T 5484-2012) is utilized for the determination of CaSO_4 quality. Instantaneous concentration of SO_2 is determined by flue gas analyzer (MRU VARIO Plus) and the average concentration of SO_2 is measured by sulfur content tester (GCS-80). The product composition is determined using XRD. Energy spectrometry (EDS, Oxford Xplore 50) and scanning electron microscopy (SEM, ZEISS Sigma 300) are employed to examine the surface morphology of PG at various phases of the reaction and under various reaction circumstances. X-ray photoelectron spectroscopy (XPS, Thermo Scientific K-Alpha) is employed to examine the valence of compounds. The test is repeated three times for each sample to minimize experimental errors. The computations are carried out as follows:

$$\varphi_{\text{CaSO}_4} = 1 - \frac{m_t \times x_{t,\text{CaSO}_4}}{m_o \times x_{o,\text{CaSO}_4}} \times 100\% \quad (1)$$

Table 4

The working conditions for the experiment.

Number	Composition	Temperature / °C	Thermostatic time / min
1	$\text{Fe}_3\text{O}_4/\text{Ca} = 0, 0.2, 0.4, 0.6, 0.8$	1100	24
2	$\text{C}/\text{Ca} = 0, 0.1, 0.2, 0.3, 0.4, 0.5$	1100	24
3	$\text{Fe}_3\text{O}_4:\text{C}:\text{Ca} = 0.6:0.4:1$	950–1100	24
4	$\text{Fe}_3\text{O}_4:\text{C}:\text{Ca} = 0.6:0.4:1$	1100	0–24

$$q_{\text{SO}_2} = \frac{F}{1000} \times \frac{c_t \times 64 \times t}{22.4} \quad (2)$$

$$\phi_{\text{SO}_2} = \frac{q_{\text{SO}_2}}{Q_{\text{SO}_2}} \times 100\% \quad (3)$$

where: φ_{CaSO_4} - decomposition ratio of PG, %. m_o - the quality of raw, g. m_t - quality of products, g. x_{t,CaSO_4} , x_{o,CaSO_4} - CaSO_4 content of the products and raw materials, %. q_{SO_2} - the production of SO_2 , g. F - the overall rate of gas flow, Nm^3/min . c_t - an average SO_2 concentration, ppm. ϕ_{SO_2} - mass yield of SO_2 , %. Q_{SO_2} - the quality of SO_2 released by the complete decomposition of CaSO_4 of PG, g.

2.4. Non-isothermal thermogravimetric experiment and thermodynamic calculations

On a thermogravimetric analyzer (Netzsch STA 449 F3), non-isothermal thermogravimetric studies are conducted. The samples are heated to 1200 °C from 30 °C with 10, 15 and 20 °C/min. N_2 is employed as the protective gas with 40 mL/min. The multiple heating ratio method is applied to reveal kinetic mechanisms, including the activation energy (E_a), the finger-forward factor ($\ln A$) and mechanism function. The two analytical methods is used include Kissinger-Akahira-Sunose (KAS) equation and Flynn-Wall-Ozawa (FWO) equation.

Relying on Gibbs free energy minimization concept, the equilibrium module in the HSC Chemistry 6.0 program is used to compute the reaction equilibrium composition. The equilibrium composition of the physical phase mainly depends on the input mixture system. To examine

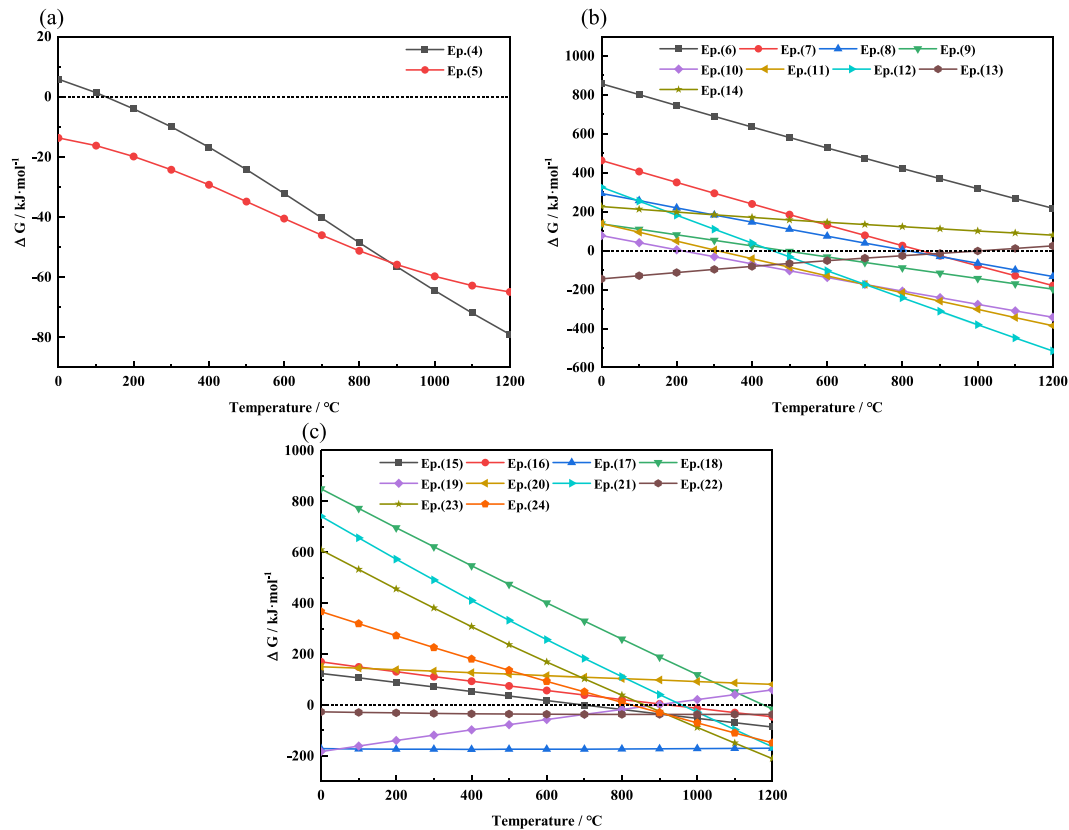


Fig. 3. Gibbs free energy of the reaction.

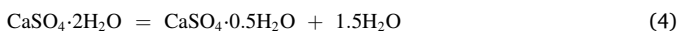
how temperature and composition affect the equilibrium composition, CaSO_4 is set to be 2 kmol, pressure to be 0.1 MPa, temperature to be 800–1100 $^{\circ}\text{C}$, C/ Ca molar ratio to be 0–1, and Fe_3O_4 / Ca molar ratio to be 0–1. Table 4 gives all the working conditions in this study.

3. Results and discussion

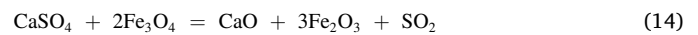
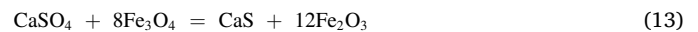
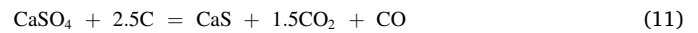
3.1. Reaction equilibrium calculations

Reaction equilibrium calculations provides an understanding of the conditions under which reactions proceed spontaneously, but also the composition of the products at reaction equilibrium, can evaluate the direction and limitations of the reactions. The reactions that may occur during CD-assisted coke reduction of PG are categorized and examined. The main reactions include (1) PG dehydration reaction, (2) PG self-decomposition and reduction reaction and (3) products continuation reaction. The specific reactions are shown below:

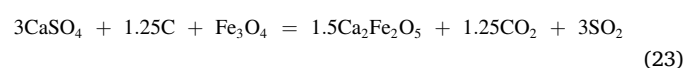
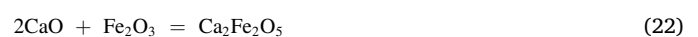
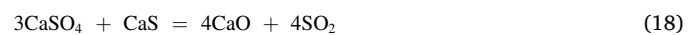
11) PG dehydration reactions



21) PG self-decomposition and reduction reactions



31) The products continue to react



The Gibbs free energies of the above reactions at 0–1200 $^{\circ}\text{C}$ are calculated using HSC. As demonstrated in Fig. 3(a), the dehydration process of PG begins to occur spontaneously at 108 $^{\circ}\text{C}$. The loss of 1.5 water of crystallization from $\text{CaSO}_4 \cdot 2\text{H}_2\text{O}$ typically takes place between

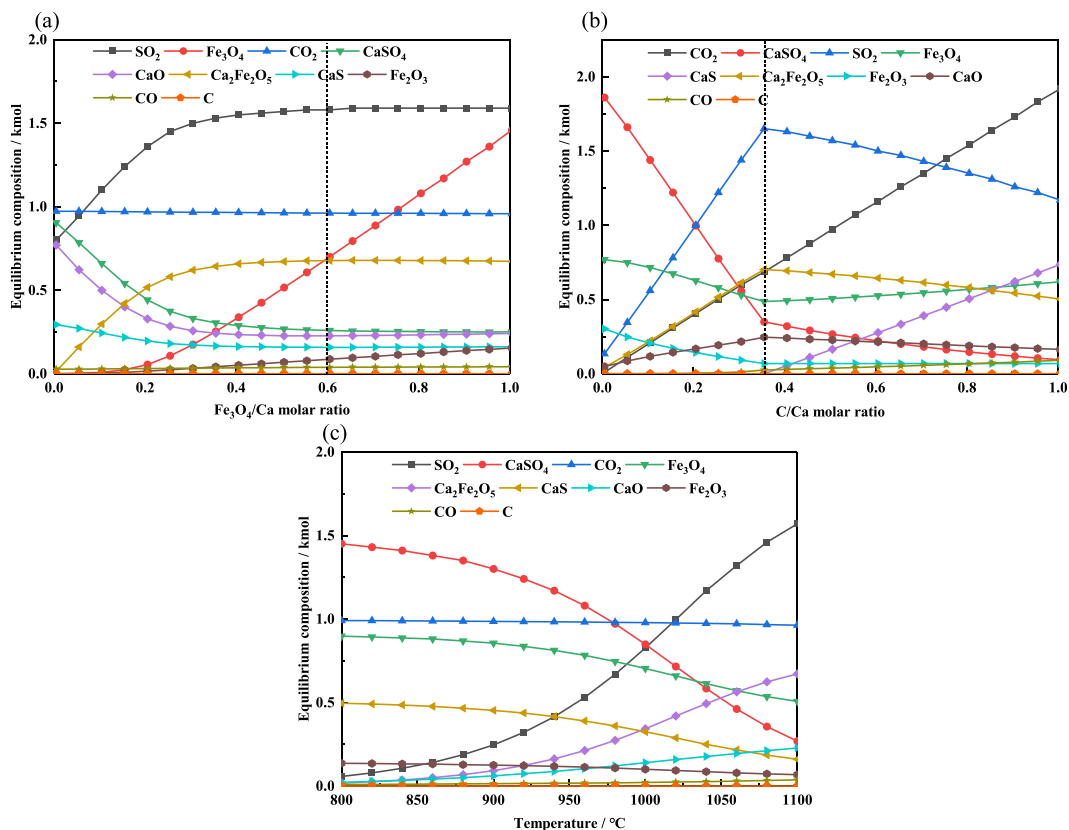


Fig. 4. Equilibrium product composition under various situations: (a) Fe₃O₄/Ca, (b) C/Ca, (c) reaction temperature.

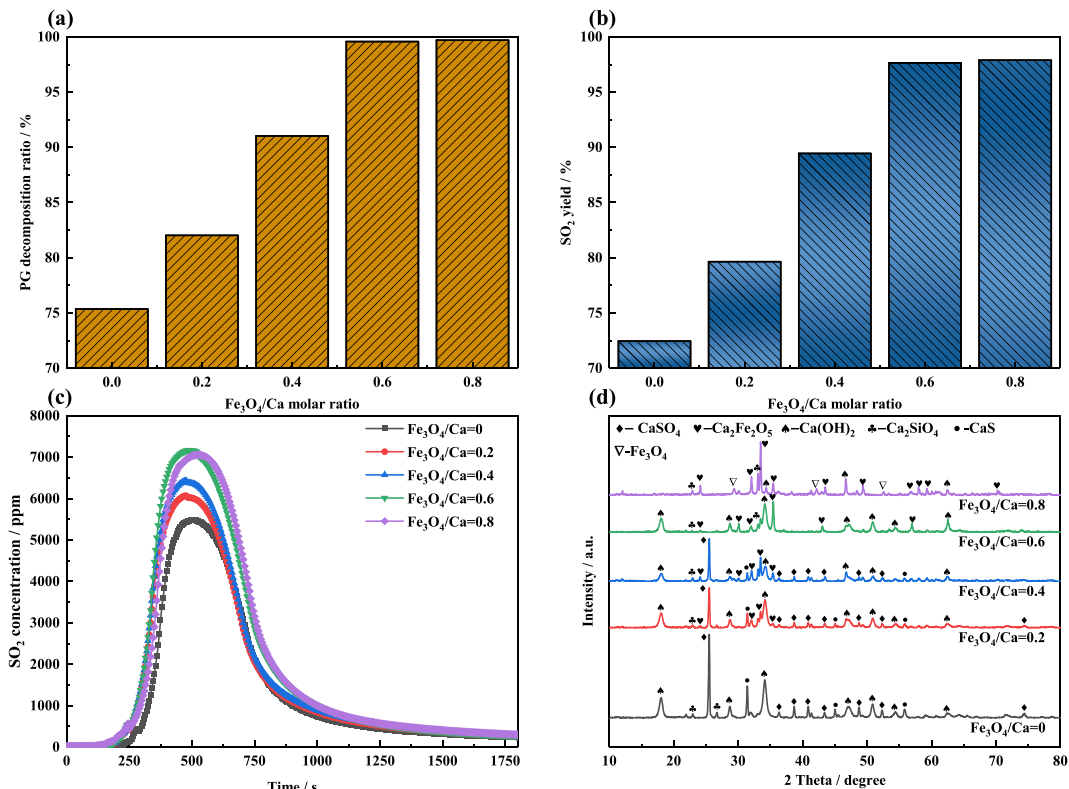


Fig. 5. Influence of Fe₃O₄/Ca on products composition: (a) PG decomposition ratio, (b) SO₂ yield, (c) SO₂ concentration with time, (d) XRD patterns of products.

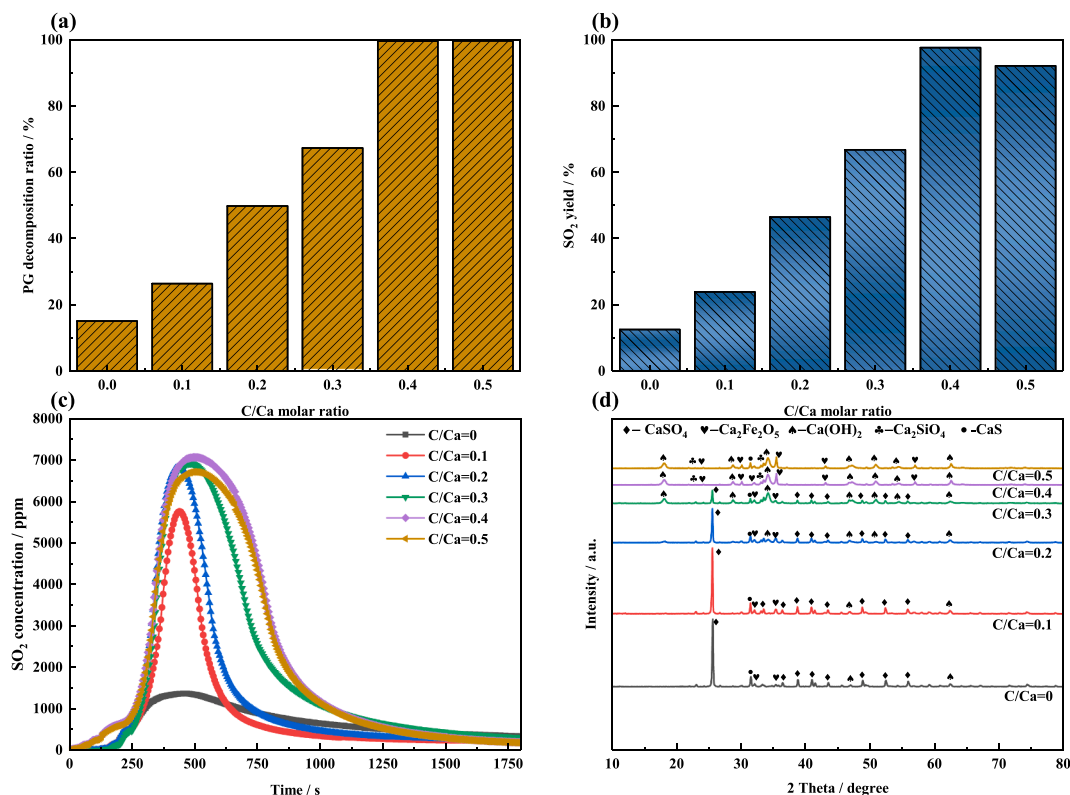


Fig. 6. Influence of C/Ca on products composition: (a) PG decomposition ratio, (b) SO₂ yield, (c) SO₂ concentration with time, and (d) XRD patterns of products.

105 °C and 145 °C. The loss of 0.5 water of crystallization from CaSO₄·0.5H₂O typically takes place between 145 °C and 185 °C (Wang et al., 2021). The thermodynamic analysis results are slightly lower than the actual occurrence temperature. From Fig. 3(b), the temperature at which CaSO₄ self-decomposes is substantially greater than 1200 °C (Li et al., 2009). The temperature at which CaSO₄ decomposes is dramatically lowered by the addition of carbon. The reduction result is mostly CaS when the C/Ca is higher than or equal to 1.5, while it is primarily CaO when the C/Ca is less than or equal to 1. CaO is mostly produced at high temperatures (900–1200 °C), which is much higher than the temperature at which CaS is produced (600–800 °C). Additionally, the additive Fe₃O₄ can take part in the reduction of CaSO₄, significantly lowering the PG initial reaction temperature. The reduction products are CaS, CaO, and Fe₂O₃. From Fig. 3(c), the reduction products can still participate in the process at high temperatures. As the main reaction of SO₂ generation, the spontaneous reaction temperature of Eq. (18) is as high as 1200 °C, and the addition of additive Fe₃O₄ significantly reduces the reaction temperature to 900–1100 °C, as shown in Eqs. (22) ~ 24, so that more SO₂ can be generated at lower temperatures. In summary, Fe₃O₄ considerably promoting the PG reduction reaction and produces more SO₂.

The effects of various parameters (Fe₃O₄/Ca, C/Ca, reaction temperature) on the reduction reaction process of CaSO₄ are further estimated using HSC in order to further define the optimum experimental settings. The CaSO₄ content is gradually dropping and the SO₂ content is gradually rising as the Fe₃O₄/Ca rising from 0 to 0.6 at 1100 °C with the C/Ca of 0.4, as can be observed in Fig. 4(a). The declining trend of CaSO₄ is no longer noticeable when the Fe₃O₄/Ca continues to increase. This shows that Fe₃O₄ can greatly speed up the process of CaSO₄ reduction reaction and favor SO₂ production. The impact of increasing the C/Ca on the reduction reaction of CaSO₄ at 1100 °C with Fe₃O₄/Ca of 0.6 can be seen in Fig. 4(b). Carbon has two effects on the process. First, when C/Ca is 0–0.4, the principal CaSO₄ reduction products are Ca₂Fe₂O₅, CaO, SO₂, CO, and CO₂. Increasing C/Ca at this point might

dramatically raise the SO₂ concentration. CaS, Ca₂Fe₂O₅, SO₂, CO, and CO₂ are the primary reduction products of CaSO₄ when C/Ca is larger than 0.4. At this point, boosting C/Ca causes more CaS to be produced while decreasing SO₂ content. Therefore, C/Ca must be kept within a range of 0.4 to produce the desired product SO₂. From Fig. 4(c), the temperature has a considerable impact on CaSO₄ reduction process. The reduction of CaSO₄ can be greatly acceleration by an increase in temperature. In conclusion, the optimal Fe₃O₄/Ca, C/Ca, and reaction temperatures are 0.6, 0.4, and 1100 °C, respectively.

3.2. Influence of Fe₃O₄/Ca

On the basis of thermodynamic calculations, a series of PG high-temperature reduction experiments are carried out. The effect of Fe₃O₄/Ca molar ratio on the decomposition process of PG is firstly investigated at 1100 °C with a C/Ca molar ratio of 0.4, and the results are shown in Fig. 5. From Fig. 5(a) and 5(b), the decomposition ratio rises from 75.35 % to 99.56 % and the SO₂ mass yield rises from 72.45 % to 97.64 % with an increase in Fe₃O₄/Ca from 0 to 0.6. The decomposition ratio at Fe₃O₄/Ca of 0.8 is not much different from that at 0.6. Fig. 5(c) shows the fluctuation in SO₂ concentration with thermostatic time. The reaction ends at around 24 min and the SO₂ concentration reaches its maximum value at around 8 min. The maximum SO₂ concentration rises from 5472 ppm to 7167 ppm with Fe₃O₄/Ca rising from 0 to 0.6. This result can also indicate that CD promotes PG decomposition leading to more SO₂ production. Continuing to increase the Fe₃O₄/Ca, the maximum concentration of SO₂ changes less. The aforementioned findings show that increasing CD addition can effectively encourage the breakdown of PG to produce SO₂. The optimized Fe₃O₄/Ca molar ratio is about 0.6. The findings accord well with the thermodynamic estimates.

The products are analyzed in physical phase as shown in Fig. 5(d). When no CD is present, the principal decomposition products are CaS, CaO, and Ca₂SiO₄. Ca(OH)₂ is formed by the reaction of CaO with

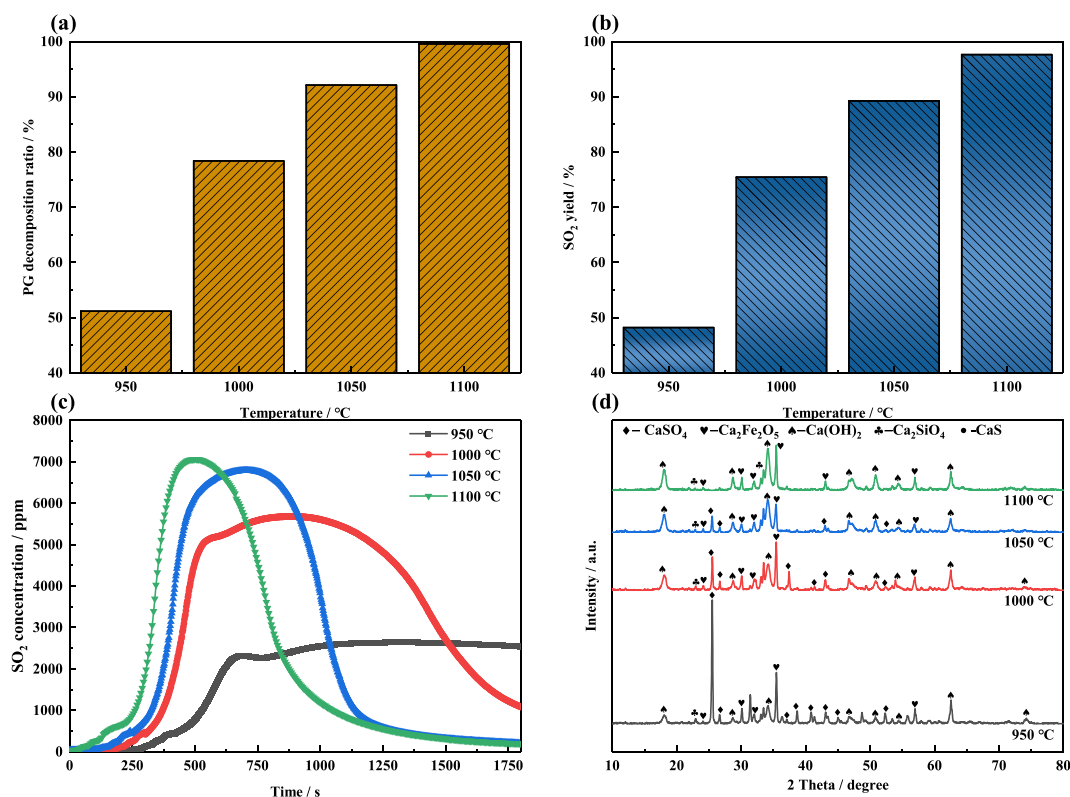


Fig. 7. Influence of temperature on products composition: (a) PG decomposition ratio, (b) SO₂ yield, (c) SO₂ concentration with time, (d) XRD patterns of products.

airborne water vapor. Ca₂SiO₄ is formed by the product CaO and the impurity SiO₂ in PG (Yang et al., 2011). The addition of CD significantly reduces the characteristic peak intensity of CaSO₄ and a new material Ca₂Fe₂O₅ emerges. The CaSO₄ phase has totally gone when Fe₃O₄/Ca is adjusted to 0.6, which indicates that PG has been decomposed completely. Continuing to increase the CD dosage, unreacted Fe₃O₄ appears in the product. This result verifies the conclusions of Fig. 4(a) and 4(b).

3.3. Influence of C/Ca

Then the effect of C/Ca molar ratio on the PG decomposition process is investigated at 1100 °C with Fe₃O₄/Ca molar ratio of 0.6, and the results are shown in Fig. 6. From Fig. 6(a) and 6(b), decomposition ratio rises from 15.12 % to 99.56 % and the SO₂ mass yield rises from 12.54 % to 97.64 % with a change in C/Ca from 0 to 0.4. The addition of coke

greatly facilitates CaSO₄ decomposition leading to more SO₂ generation. However, the yield of SO₂ falls to 92.12 % as C/Ca rising to 0.6. This is mainly caused by the generation of CaS as a by-product. This result can also be seen in Fig. 6(c). When no carbon is added, the highest SO₂ concentration is just 1370 ppm, but this grows dramatically when carbon is introduced. As C/Ca rising from 0.4 to 0.5, the maximum value of SO₂ concentration decreases from 7167 ppm to 6712 ppm.

The products are submitted to phase transition analysis to clarify the impact of carbon on the process, and the findings are presented in Fig. 6(d). The strength of CaSO₄ peaks steadily diminish as the carbon concentration increases. Moreover, CaS can still be seen when no carbon is injected. Since CaS is produced by the PG reduction process, this indicates that Fe₃O₄ in CD can also participate in the PG reduction process. This result verifies the previous thermodynamic calculations. As C/Ca growing from 0.1 to 0.4, the strength of the distinctive peaks of CaS in the intermediate product progressively diminishes, while the intensity

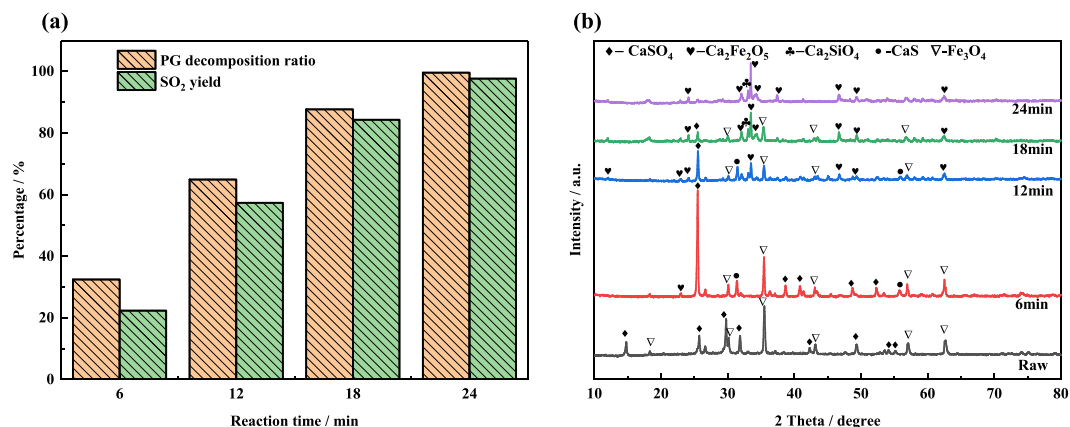


Fig. 8. Influence of thermostatic time on product composition: (a) SO₂ yield and decomposition ratio, (b) XRD pattern of products.

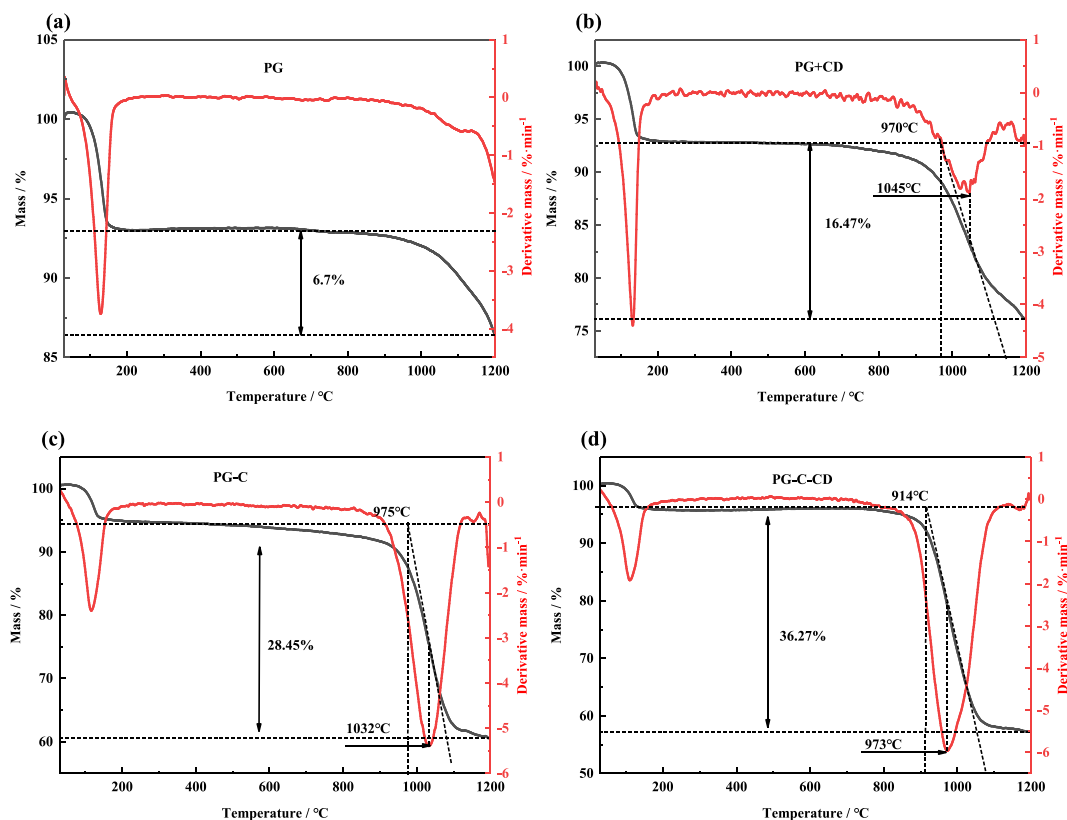


Fig. 9. TG-DTG curves: (a) PG alone, (b) $\text{Fe}_3\text{O}_4/\text{Ca} = 0.6$, (c) $\text{C}/\text{Ca} = 0.4$, (d) $\text{Fe}_3\text{O}_4/\text{Ca} = 0.6$, $\text{C}/\text{Ca} = 0.4$.

of the $\text{Ca}_2\text{Fe}_2\text{O}_5$ steadily increases. Continuing to increase the carbon content, the obvious CaS characteristic peaks appears again in the product. The SO_2 yield is reduced due to CaS production. In summary the optimized C/Ca is 0.4.

3.4. Influence of temperature

The thermodynamic calculations above reveals that temperature has a large effect on the process. Therefore the effect of temperature on the PG decomposition process is examined at a C/Ca molar ratio of 0.4 and $\text{Fe}_3\text{O}_4/\text{Ca}$ molar ratio of 0.6, and the results are shown in Fig. 7. As shown in Fig. 7(a) and 7(b), raising the temperature greatly increases the decomposition ratio and SO_2 mass yield. The decomposition ratio rises from 51.18 % to 99.56 % and the SO_2 mass yield rises from 48.21 % to 97.64 % from 950 °C to 1100 °C. Fig. 7(c) shows the curve of SO_2 concentration throughout time. At 950 °C, the reaction remains unfinished after 30 min. As the temperature increasing, the release time of SO_2 becomes more advanced and the maximum concentration of SO_2 is increasing. At the same time, the time required for the reaction is also scaled down. This suggests that increasing the temperature hastens the ratio of SO_2 emission from PG degradation. The results of the physical phase analysis are given in Fig. 7(d). CaSO_4 intensity decreases as temperature increasing, while the intensity of $\text{Ca}_2\text{Fe}_2\text{O}_5$ and $\text{Ca}(\text{OH})_2$ increasing, indicating that PG decomposition is more favorable at higher temperatures. In summary, the optimal reaction temperature for obtaining the desired product SO_2 is 1100 °C.

3.5. Influence of thermostatic time

Finally, the effect of reaction time on the PG decomposition process is investigated at a C/Ca molar ratio of 0.4, $\text{Fe}_3\text{O}_4/\text{Ca}$ molar ratio of 0.6 at 1100 °C, and the results are shown in Fig. 8. From Fig. 8(a), as the reaction duration extending from 6 to 24 min, the decomposition ratio

climbs from 32.47 % to 99.56 %, and the SO_2 mass yield climbs from 22.32 % to 97.64 %. From Fig. 8(b), CaSO_4 in PG is decomposed into the intermediate product CaS, resulting in the sulfur in the CaSO_4 is not completely converted to SO_2 at 6 min. The characteristic peak of CaSO_4 disappears as the thermostatic time increases. This is due to the production of SO_2 and CaO from the roasting reaction between CaSO_4 and CaS at high temperatures (Min et al., 2009). Furthermore, the CaSO_4 progressively oxidizes the Fe_3O_4 to $\text{Ca}_2\text{Fe}_2\text{O}_5$, and the process releases SO_2 . In summary, the optimized thermostatic time is 24 min.

3.6. Thermogravimetric experiments

The thermogravimetric behaviors of PG alone (a), $\text{Fe}_3\text{O}_4/\text{Ca} = 0.6$ (b), $\text{C}/\text{Ca} = 0.4$ (c) and $\text{Fe}_3\text{O}_4/\text{Ca} = 0.6$, $\text{C}/\text{Ca} = 0.4$ (d) are investigated in the range of 30–1200 °C by using a thermogravimetric analyzer. Fig. 9 (a) shows the thermogravimetric curves of PG alone. It can be shown that the initial decomposition temperature of PG alone is about 1000 °C. It is much lower than the thermodynamic predictions, which might be attributed to SiO_2 in PG reducing the temperature (Yan et al., 2015). The weight loss of PG at this stage is only 6.7 %. Fig. 9(b) shows the thermogravimetric curve at $\text{Fe}_3\text{O}_4/\text{Ca} = 0.6$. There are two distinct phases of weight loss in this sample. The first occurs at 105–180 °C, which is a water loss reaction of $\text{CaSO}_4 \cdot 2\text{H}_2\text{O}$. The second occurs at 970–1200 °C, which is the carbon reduction of PG to produce CaS and CaO, while SO_2 , CO_2 and CO gases are released. The weight loss of this process is 16.47 %, and the temperature associated with the greatest weight loss is 1045 °C. This indicates that Fe_3O_4 in CD also significantly promotes the decomposition of PG to produce SO_2 . Fig. 9(c) shows the thermogravimetric curve at $\text{C}/\text{Ca} = 0.4$. The total weight loss trend of the curve does not change, but the weight loss at this stage is 28.45 %, which is significantly higher than that of 16.47 % for CD, which indicates that the decomposition effect of coke is significantly stronger than that of CD. Fig. 9(d) shows the thermogravimetric curves at $\text{Fe}_3\text{O}_4/\text{Ca} = 0.6$ and $\text{C}/$

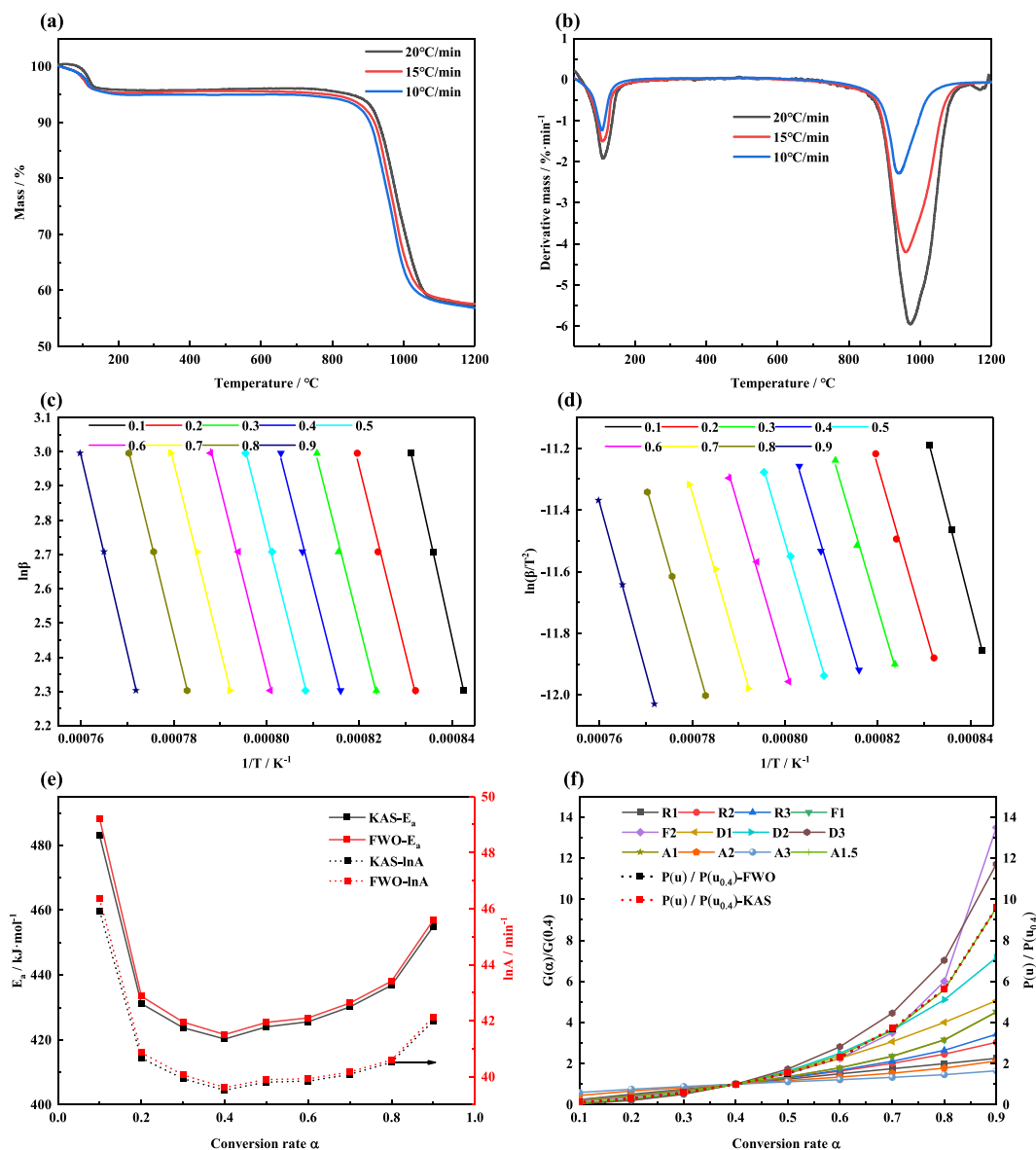


Fig. 10. Dynamics calculation.

Ca = 0.4. When compared to Fig. 9(c), the beginning temperature of the second weight loss process drops from 975 °C to 914 °C, the weight loss increases from 28.45 % to 36.27 %, and the highest weight loss temperature drops from 1032 °C to 973 °C. This study also implies that Fe₃O₄ in CD can contribute in the decomposition reaction, decreasing the decomposition temperature while also boosting PG decomposition to create SO₂.

Non-isothermal thermogravimetric studies are carried out to disclose the kinetic mechanism of the process. To disclose the reduction law, the kinetic parameters are estimated at different conversion ratios from 900 to 1100 °C using the FWO and KAS, respectively. Since CD-assisted coke reduction of PG is a complex multiphase reaction system, which includes gas–solid and solid–solid reactions, several common kinetic mechanism functions are selected for the calculations in this paper (Liu et al., 2023). As shown in Table S1, the specific calculation procedures are described in the supporting information. Fig. 10(a) and 10(b) illustration the TG-DTG curves at various heating ratios. The TG curves demonstration that curved line changes further toward the high temperature end the faster the heating rate. Thermogravimetric curve has an obvious temperature lag effect. The DTG curve shows that the higher the heating ratio, the more the DTG peak of the PG breakdown process shifts to the high

temperature end, and the greater the peak value. The fitted curves derived by the FWO approach are shown in Fig. 10(c). The fitted curves derived by the KAS approach are shown in Fig. 10(d). The E_a and lnA at different conversion ratios are derived after conversion, as shown in Fig. 10(e). E_a generation from both approaches reduces and then grows as the conversion ratio increases, reaching the minimum value at 0.4. Therefore, the conversion ratio of 0.4 is chosen as the reference point of the interval, and the difference between the integral curve functional equation and the given solid mechanism functional equation is compared, as shown in Fig. 10(f). By fitting, the final most-solids mechanism function for the CD-assisted reduction of the PG process is obtained as $G(\alpha) = [-\ln(1-\alpha)]^{3/2}$, indicating that the decomposition reaction mechanism is a crystal nucleation and growth-controlled process (Yang et al., 2016).

3.7. Microanalysis

According to the results above, temperature, C/Ca and Fe₃O₄/Ca have a strong influence on the PG decomposition process. Elevating the temperature and Fe₃O₄/Ca, as well as managing the optimum C/Ca, may greatly speed up the decomposition reaction to produce SO₂. The

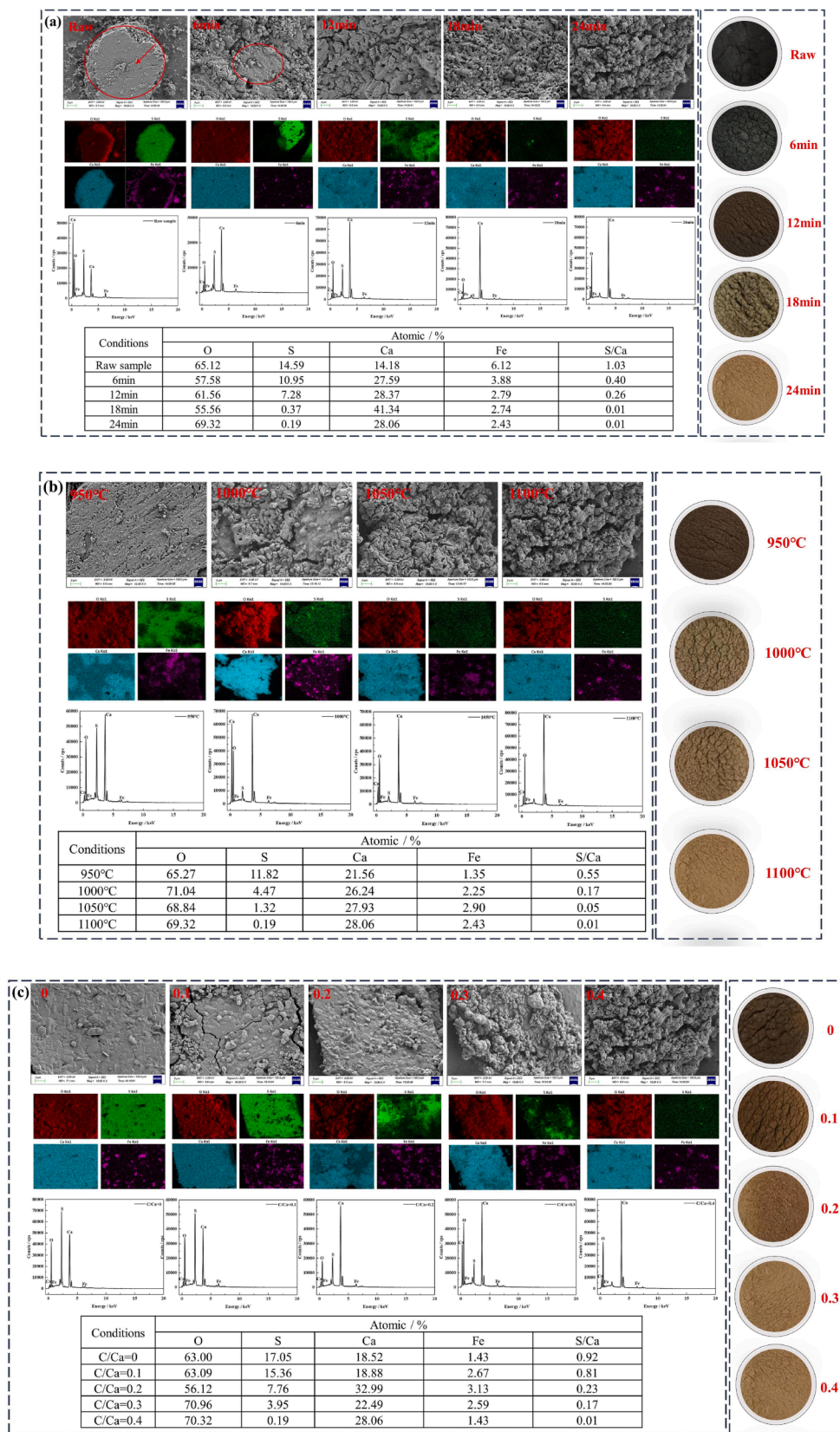


Fig. 11. SEM-EDS of the samples under different conditions: (a) thermostatic time, (b) reaction temperature, (c) C/Ca, (d) Fe₃O₄/Ca.

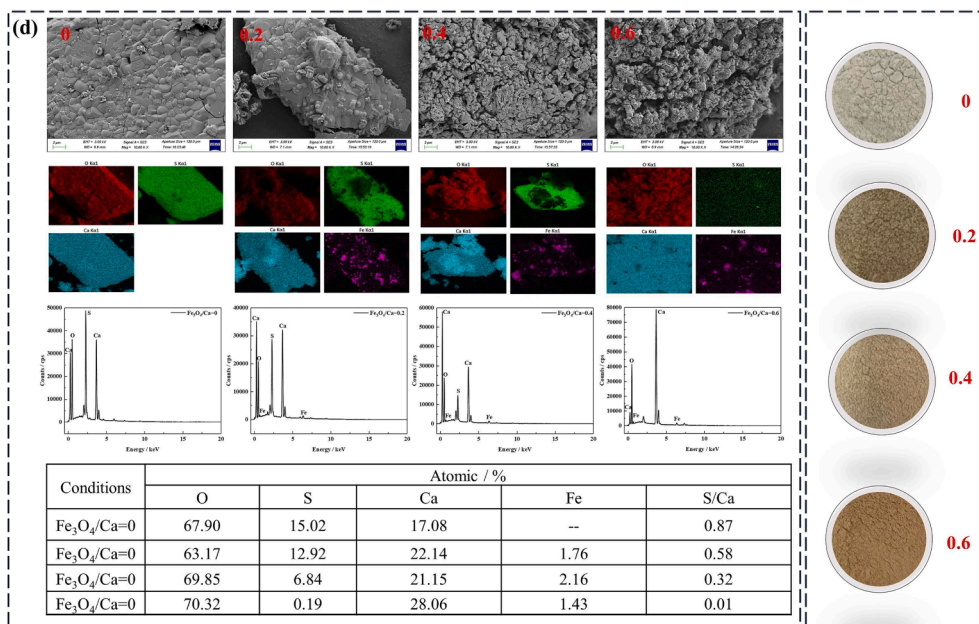


Fig. 11. (continued).

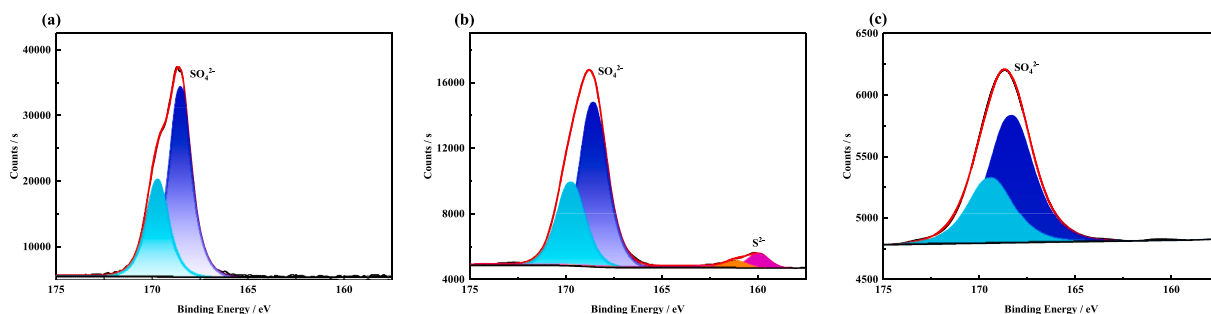


Fig. 12. XPS profiles of products at different thermostatic times: (a) raw material, (b) 6 min, (c) 18 min.

products are evaluated by SEM-EDS to further illustration the good impacts.

From Fig. 11(a), the surface of the raw material is relatively smooth before the reaction starts, when the reaction is 6 min, the material becomes rough and uneven around, and the center still consists of smooth surface. The surface of the material gets fully rough after 12 min. As thermostatic time continues to increase, the surface of the material

shows many uniform and dense small particles. The figure show that the reaction begins at the border. As thermostatic time increases, the reaction diffuses from outside to inside, eventually nucleating. This finding is consistent with the kinetic estimates shown above. In addition, the S/Ca atomic ratio is calculated by EDS. The S/Ca atomic ratio falls from 1.03 to 0.01 as thermostatic time increasing, which indicates that the CaSO₄ in PG is completely decomposed into SO₂. In addition, the material

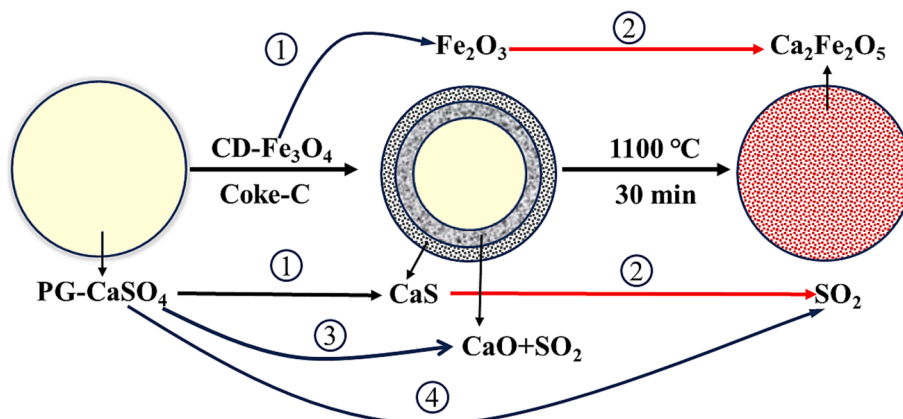


Fig. 13. Reaction mechanism.

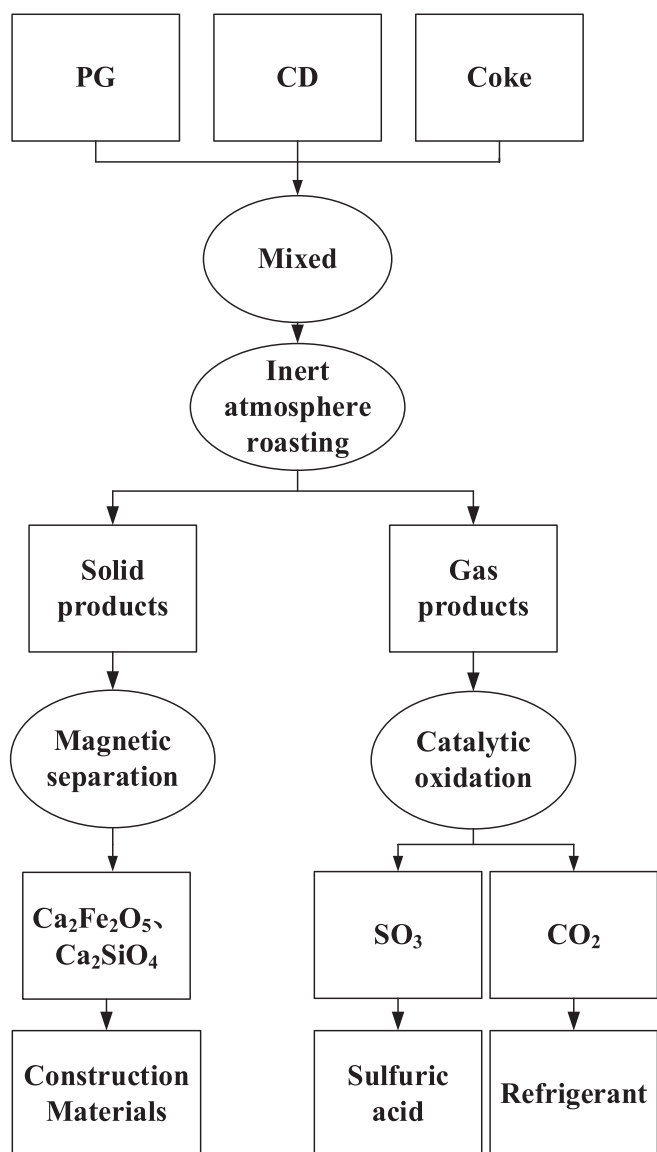


Fig. 14. Process flow diagram for SO_2 production from CD synergistic coke decomposition PG.

gradually changes from black to light red, which indicates that the Fe_3O_4 in CD is gradually oxidized to $\text{Ca}_2\text{Fe}_2\text{O}_5$.

Fig. 11(b) depicts the surface properties of the material at various temperatures. The material's surface is quite smooth at 950°C , as can be observed. With the increase of temperature, the material's surface roughens and becomes uneven. Furthermore, this process is extended from the boundary to the center. Combined with the EDS plot, S/Ca drops from 0.55 to 0.01 with the temperature increasing, showing that increasing temperature enhances the breakdown of CaSO_4 in PG to form SO_2 . In addition, the material undergoes transformation from dark black to light red, indicating that Fe_3O_4 in CD is oxidized to generation $\text{Ca}_2\text{Fe}_2\text{O}_5$.

Fig. 11(c) depicts the surface characteristics of the materials at various C/Ca. When the C/Ca is 0, the material's surface is smooth. The surface of the material becomes honeycomb as the C/Ca increases. When the C/Ca is 0.4, the surface of the material becomes rough and uneven. Combined with EDS, S/Ca reduces from 0.92 to 0.01, demonstrating that increasing coke presence is beneficial to the decomposition process. Furthermore, the surface of the material is transformed from dark black to light red, indicating that the valence state transition of Fe_3O_4 in CD occurs.

The surface characteristics of the materials at various $\text{Fe}_3\text{O}_4/\text{Ca}$ are shown in Fig. 11(d). When no CD is added, the material is composed of a honeycomb surface. With the addition of CD, the surface of the material changes dramatically, and a small uniform particle begins to protrude, which indicates that the Fe_3O_4 in CD has a role in the PG reaction pathway. Combined with the EDS plot, S/Ca declines from 0.87 to 0.01 as $\text{Fe}_3\text{O}_4/\text{Ca}$ increasing, indicating that an increase in Fe_3O_4 is beneficial to the decomposition process.

The products are then subjected to XPS analysis. The fitting of unreacted CaSO_4 to S 2p is shown in Fig. 12(a). S $2p^{3/2}$ has the binding energy of 169.22 eV, which relates to SO_4^{2-} in CaSO_4 (Ghahremaninezhad et al., 2013). Fig. 12(b) shows fitting of the product of S 2p after 6 min. A new double state occurs on the spectrum with the binding energy of 160.33 eV, which relates to S^{2-} . (Yang et al., 2018) Fig. 12(c) shows the fit to the product of S 2p after 18 min. It can be seen that S^{2-} disappears from the spectrum and only SO_4^{2-} remains. This suggests that CaS is a reaction intermediate.

3.8. Reaction mechanism

In summary, the reaction mechanism for the process is proposed as shown in Fig. 13. The process is composed of four parts. (1) CaSO_4 in PG is first reduced to the intermediate product CaS by Fe_3O_4 in CD, while Fe_3O_4 is oxidized to Fe_2O_3 . (2) At high temperature, CaS and CaSO_4 is still reacting with Fe_2O_3 to form $\text{Ca}_2\text{Fe}_2\text{O}_5$ and SO_2 . The addition of Fe_2O_3 hastens the roasting process of CaS and CaSO_4 and lowers the reaction temperature. (3) Coke reduces CaSO_4 to CaS , which then reacts with CaSO_4 to form SO_2 and CaO . (4) CaSO_4 in PG partially decomposes to form SO_2 and CaO .

Finally, a process for producing SO_2 utilizing CD breakdown of PG is developed, which may remove PG pollution while producing chemical products such as SO_2 , Ca_2SiO_4 , and $\text{Ca}_2\text{Fe}_2\text{O}_5$. The process is illustrated in Fig. 14. The process consists of three main steps, which are raw material proportioning, high temperature roasting and products separation. (1) Material proportion. Based on the results of the above experiments, $\text{Fe}_3\text{O}_4/\text{Ca}$ of 0.6, C/Ca of 0.4 is the optimized ratio. (2) High temperature roasting. PG could be completely decomposed and SO_2 is obtained in 97.64 % yield at 1100°C for 24 min. In addition, the by-products Ca_2SiO_4 and $\text{Ca}_2\text{Fe}_2\text{O}_5$ could be produced. (3) Products separation. $\text{Ca}_2\text{Fe}_2\text{O}_5$ and Ca_2SiO_4 can be used as building materials. Some well-established catalysts, such as V_2O_5 (Ma et al., 2008), are used to convert SO_2 to SO_3 , which is used to continue the production of sulfuric acid. This allows the separation of SO_2 from CO_2 . CO_2 can be used as a refrigerant.

4. Conclusion

In this paper, a process for the preparation of SO_2 from solid waste CD as a novel additive to assist coke reduction of PG was proposed. To optimize process conditions, the impacts of raw material ratios, roasting time and temperature on the process were explored using fluidized bed tests. It turns out that the optimized reaction conditions for obtaining the target product SO_2 are $\text{Fe}_3\text{O}_4/\text{Ca}$ of 0.6, C/Ca of 0.4 at 1100°C for 24 min, under which the PG decomposition ratio and SO_2 mass yield are 99.56 % and 97.64 %, respectively. The incorporation of CD is able to lower the initial reaction of PG-coke system temperature from 975°C to 914°C and facilitates CaSO_4 decomposition to produce SO_2 . Kinetic analysis shows the mechanistic equation for this process is obtained as $G(\alpha) = [-\ln(1-\alpha)]^{3/2}$, indicating that the decomposition reaction mechanism is a crystal nucleation and growth-controlled process. The mechanism of the process is that CaSO_4 is converted to the intermediate product CaS by Fe_3O_4 and coke. Meanwhile, Fe_3O_4 is oxidized to Fe_2O_3 . At high temperatures, CaS and CaSO_4 is still reacting with Fe_2O_3 to form $\text{Ca}_2\text{Fe}_2\text{O}_5$ and SO_2 . The presence of Fe_2O_3 accelerations the rate of CaS and CaSO_4 roasting reaction and reduces the reaction temperature. At the same time, CaSO_4 in PG will decompose to a certain extent to

produce CaO and SO₂ at high temperature. Finally, a process for SO₂ production from converter ash synergized with coke decomposition of PG is proposed.

Funding

Thanks for the financial supported by the Fundamental Research Funds for the Central Universities (2022ZJFH004).

CRediT authorship contribution statement

Dong Ma: Writing – original draft, Writing – review & editing. **Qinhui Wang:** Writing – review & editing. **Zhihua Tian:** Writing – review & editing. **Bin Zhang:** Writing – review & editing. **Guilin Xie:** Writing – review & editing.

Declaration of competing interest

The authors declare the following financial interests/personal relationships which may be considered as potential competing interests: Qinhui Wang reports financial support was provided by The Fundamental Research Funds for the Central Universities.

Data availability

No data was used for the research described in the article.

Appendix A. Supplementary data

Supplementary data to this article can be found online at <https://doi.org/10.1016/j.ces.2024.119814>.

References

- Atanasova, L.G., 2010. Exergy analysis of the process of wet-process phosphoric acid production with full utilisation of sulphur contained in the waste phosphogypsum. *Int. J. Exergy* 7, 678–692.
- Chen, S., Chen, J.Z., He, X.Y., Su, Y., Jin, Z.H., Fan, J.Y., Qi, H.H., Wang, B., 2023. Comparative analysis of colloid-mechanical microenvironments on the efficient purification of phosphogypsum. *Constr. Build. Mater.* 392.
- Chen, Y., Wang, C., Zhao, B., Yao, Y., 2021. Preparation of sulphoaluminate cement by pre-reduction of phosphogypsum with gas sulfur. *Non-Metallic Mines* 44, 9–12.
- Da Rocha EP, De Castro JA, Araujo GM and Martins L, Characterization of BOF dust for pellets production used in blast furnace, in 57th Brazilian Ceramic Conference (CBC), Natal, BRAZIL, pp. 611–616 (2013).
- Ennaciri, Y., Bettach, M., 2018. Procedure to convert phosphogypsum waste into valuable products. *Mater. Manuf. Process.* 33, 1727–1733.
- Ennaciri, Y., Bettach, M., El Alaoui-Belghiti, H., 2020. Recovery of nano-calcium fluoride and ammonium bisulphate from phosphogypsum waste. *Int. J. Environ. Stud.* 77, 297–306.
- Fang, R., Tan, H.B., Mao, W.J., Ma, X.L., Feng, Y., Jiang, Q., Yang, F.H., 2020. Influence of carbon and additives on the high-temperature decomposition behavior of phosphogypsum. *Mater. Technol.* 54, 861–865.
- Gahremaninezhad, A., Dixon, D.G., Asselin, E., 2013. Electrochemical and XPS analysis of chalcopyrite (CuFeS₂) dissolution in sulfuric acid solution. *Electrochim. Acta* 87, 97–112.
- He, H.W., Fan, C.G., Li, S.G., Lin, W.G., 2023. Phosphogypsum decomposition by char under a CO₂ atmosphere. *Ind. Eng. Chem. Res.* 62, 9619–9628.
- Ji, L.P., Liu, Z.S., Li, Z.H., Huang, W.J., Xu, H.M., Qu, Z., Yan, N.Q., 2023. Enhanced reduction of smelting gypsum by H₂S and in-situ DRIFTS investigated on the mechanisms of S-O bond activation. *Fuel* 347.
- Jia, X., Lu, H.Y., Hui, Y., Zhang, Y.H., Han, Z.N., Wang, C., Song, X.F., Xu, G.W., 2023. Pyrolyzing coal blended with ash: The fate and impacts of CaSO₄. *J. Anal. Appl. Pyrol.* 169.
- Li, J., Yu, S., Ma, L., Shu, Y., Tang, S., Lu, K., Zhang, P., Cao, Y., 2009. Thermal analysis of phosphogypsum decomposition. *Chin. J. Environ. Eng.* 3, 1861–1864.
- Liu, L.C., Fan, X.H., Gan, M., Sun, Z.Q., Ji, Z.Y., Wei, J.Y., Liu, J.Y., 2023. Advances on resource utilization of semi-dry desulfurization ash by thermal decomposition: a high-efficiency and low-temperature method for large-scale processing. *Environ. Sci. Pollut. Res.*
- Liu, S., Yang, C.R., Zhang, T.F., Liu, W., Jiao, F., Qin, W.Q., 2023. Effective recovery of calcium and sulfur resources in FGD gypsum: Insights from the mechanism of reduction roasting and the conversion process of sulfur element. *Sep. Purif. Technol.* 314.
- Liu, H., Sulfur-containing gas, Calcium carbonate and iron concentrate by phosphogypsum and pyrite production involves mixing phosphogypsum and pyrite to conduct two-stage roasting to obtain sulfur-containing gas and roast slag. CN111118280-A; CN111118280-B.
- Lu, D.H., Chen, Q.L., Li, C.Q., Gong, S., 2021. Effect of potassium feldspar on the decomposition rate of phosphogypsum. *J. Chem. Technol. Biotechnol.* 96, 374–383.
- Luo, Q., Deng, Q.L., Liao, H.W., Wang, W.J., Zeng, B.L., Luo, C.L., Tu, J.H., Wu, L.X., Tan, H.B., Dong, F.Q., 2023. Low temperature and highly-efficient one-step decomposition of phosphogypsum via biochar by Fe³⁺/Co²⁺/Ni²⁺ unitary/ternary catalyst. *Environ. Sci. Pollut. Res.*
- Ma, J., Liu, Z., Liu, Q., Guo, S., Huang, Z., Xiao, Y., 2008. SO₂ and NO removal from flue gas over V₂O₅/AC at lower temperatures - role of V₂O₅ on SO₂ removal. *Fuel Process. Technol.* 89, 242–248.
- Ma, D., Wang, Q.H., 2023. Experimental study on preparation of calcium oxide by coal reduction of calcium sulfate in carbon dioxide atmosphere. *J. Chem. Technol. Biotechnol.* 98, 2192–2202.
- Ma, D., Wang, Q., Tian, Z., 2023. Preparation of calcium sulfide by sludge-assisted rice husk reduction of phosphogypsum. *Asia Pac. J. Chem. Eng.* 18, e2915.
- Min, Z., Laihong, S., Zhengping, G.A.O., Jun, X., 2009. Oxidation of CaS with O₂ for oxygen carrier regeneration in chemical-looping combustion. *Acta Sci. Circumst.* 29, 330–338.
- Qi, J., Zhu, H., Zhou, P., Wang, X., Wang, Z., Yang, S., Yang, D., Li, B., 2023. Application of phosphogypsum in soilization: a review. *Int. J. Environ. Sci. Technol.*
- Shi, T., Wan, T., Zhang, Z., Yang, X., Yang, L., Zhong, B., Kong, X., Wang, X., 2016. Effect of SiO₂ on the melting characteristics of reaction between phosphogypsum and calcium sulfide. *J. Therm. Anal. Calorim.* 123, 1601–1609.
- Silva, L.F.O., Oliveira, M.L.S., Crissien, T.J., Santosh, M., Bolivar, J., Shao, L.Y., Dotto, G. L., Gasparotto, J., Schindler, M., 2022. A review on the environmental impact of phosphogypsum and potential health impacts through the release of nanoparticles. *Chemosphere* 286.
- Sun, L., Zhao, Z.J., Yang, X.S., Sun, Y., Li, Q.D., Luo, C.H., Zhao, Q., 2022. Thermochemical decomposition of phosphogypsum with Fe-P slag via a solid-state reaction. *Chin. J. Chem. Eng.* 47, 113–119.
- Wang, B.Q., Yang, L., Cao, J.X., 2021. The influence of impurities on the dehydration and conversion process of calcium sulfate dihydrate to alpha-calcium sulfate hemihydrate in the two-step wet-process phosphoric acid production. *ACS Sustain. Chem. Eng.* 9, 14365–14374.
- Yan, Z.Q., Wang, Z.A., Liu, H., Tu, Y.J., Yang, W., Zeng, H.C., Qiu, J.R., 2015. Decomposition and solid reactions of calcium sulfate doped with SiO₂, Fe₂O₃ and Al₂O₃. *J. Anal. Appl. Pyrol.* 113, 491–498.
- Yang, X., Deng, S., Huang, P., Wang, X., Yang, L., Zhang, Z., Zhong, B., 2016. Thermal analysis kinetic studies on solid-solid reaction of calcium sulfide and phosphogypsum. *J. Chem. Eng. Chin. Univ.* 30, 588–596.
- Yang CY, Wei Y, Ye FB, Ding YG and Wu YX, Effect of additives on thermal decomposition of phosphogypsum, in 2nd International Conference on Advances in Materials and Manufacturing Processes (ICAMMP 2011), Guilin, Peoples R China, pp. 735 (2011).
- Yang, C.R., Qin, W.Q., Zhao, H.B., Wang, J., Wang, X.J., 2018. Mixed potential plays a key role in leaching of chalcopyrite: experimental and theoretical analysis. *Ind. Eng. Chem. Res.* 57, 1733–1744.
- Yang, J., Zhu, B., Ma, L.P., Liu, H.P., 2019. Investigation of Al₂O₃ and Fe₂O₃ transmission and transformation during the decomposition of phosphogypsum. *Chin. J. Chem. Eng.* 27, 1125–1131.
- Zhao, L., Wan, T., Yang, X., Yang, L., Kong, X., Zhang, Z., Wang, X., 2015. Effects of kaolinite addition on the melting characteristics of the reaction between phosphogypsum and CaS. *J. Therm. Anal. Calorim.* 119, 2119–2126.
- Zheng, D., Lu, H., Sun, X., Liu, X., Han, W., Wang, L., 2013. Reaction mechanism of reductive decomposition of FGD gypsum with anthracite. *Thermochim. Acta* 559, 23–31.
- Zheng, D.L., Ma, L.P., Wang, R.M., Yang, J., Dai, Q.X., 2018. Research on thermal decomposing properties of phosphogypsum with Fe addition under multi-atmosphere control. *Thermochim. Acta* 661, 59–66.
- Zheng, S.C., Ning, P., Ma, L.P., Niu, X.K., Zhang, W., Chen, Y.H., 2011. Reductive decomposition of phosphogypsum with high-sulfur-concentration coal to SO₂ in an inert atmosphere. *Chem. Eng. Res. Des.* 89, 2736–2741.
- Zhou, Y., Zhu, R., Wei, G.S., 2022. Recent advancements in source reduction and recycling technologies for converter dust. *Energy Rep.* 8, 7274–7285.